JOURNAL OF PROPULSION AND POWER
Vol. 26, No. 4, July–August 2010

Controlling Separation on a Simulated Compressor Blade Using Vortex-Generator Jets

Simon Evans,* Howard Hodson,† Tom Hynes,‡ and Christian Wakelam§
University of Cambridge, Cambridge, England CB3 0DY, United Kingdom
and
Sven-Jürgen Hiller¶
MTU Aero Engines, GmbH, 80995 Munich, Germany

DOI: 10.2514/1.45518

Flow control using vortex-generator jets has been used to control a separating boundary layer on the surface of a flat plate in the presence of a pressure distribution equaling that on the suction surface of a compressor blade. A parametric study has been performed in which the skew angle and jet velocity of steady jets have been varied. In addition to steady blowing, the jets have been pulsed over a range of reduced frequency from 0.5 to 7.0. Steady blowing with a jet velocity greater than the inlet flow velocity was found to delay separation on the surface of the flat plate and reduce the loss coefficient of an equivalent cascade blade by 36%, relative to the unactuated case. This jet velocity is equivalent to an injected mass flow rate of 0.13% of the inlet mass flow rate. With pulsed blowing, the same loss reduction was achieved over the unactuated case using 40% less mass flow. This loss reduction, however, required a reduced frequency greater than 6.0 and a peak jet velocity equal to 1.5 times the inlet flow velocity. This corresponds to a jet Mach number in a real compressor of 1.125, pulsing at more than 180 kHz.

Nomenclature

A	=	area, m^2
b	=	span, m
C_μ	=	injected momentum coefficient,
F^+	=	reduced actuation frequency
f	=	actuation frequency, Hz
L	=	length of the separated region on the flat-plate surface, in the unactuated case, m
$\dot{m}$	=	mass flow rate, kg/s
p_0	=	stagnation pressure, Pa
s	=	effective blade pitch, m
t	=	effective trailing-edge thickness, m
V	=	velocity, m/s,
$\bar{V}$	=	mean velocity, m/s
V'	=	fluctuation velocity, from the mean, m/s
Y	=	mixed-out stagnation-to-stagnation pressure loss coefficient
α	=	flow angle, °
Γ	=	circulation, m^2/s
δ^*	=	displacement thickness, m
θ	=	momentum thickness, m
ρ	=	density, kg/m^3

Subscripts

j	=	jet
p	=	profile
x	=	axial
1	=	upstream
2	=	downstream

Presented as Paper 4317 at the 4th Flow Control Conference, Seattle, WA, 23–26 June 2008; received 15 June 2009; revision received 29 January 2010; accepted for publication 14 April 2010.

*Assistant Professor, Whittle Laboratory, Mechanical Engineering; Worcester Polytechnic Institute, 100 Institute Road, Worcester, Massachusetts 01609; sevans@wpi.edu.

†Professor of Aerothermal Technology, Whittle Laboratory, Department of Engineering, 1 JJ Thomson Avenue. Senior Member AIAA.

‡Reader, Whittle Laboratory, Department of Engineering, 1 JJ Thomson Avenue.

§Research Associate, Institute for Jet Propulsion, Universität der Bundeswehr München, 85577 Neubiberg, Germany.

¶Senior Engineer, Department of Compressor and Turbine Aerodynamics, Dachauer Street 665.

I. Introduction

VARIABLE inlet guide vanes (IGVs) and variable stator vanes extend the range of operation of a compressor by increasing their stagger angle when the compressor operates offdesign. The increased stagger angle allows the stator blades to receive the flow from upstream rotor blade rows at a reasonable incidence, and increases the exit flow angles from the stator and IGV blade rows such that incidence onto the following fixed-stagger rotor blades is not so high as to cause flow separation from the suction surfaces of the airfoils. The disadvantage of such a system, however, is the complexity of the variable geometry and the weight of the drive system required to operate it. These systems can weigh as much as two passengers on a large twin-engine wide-body aircraft. It is therefore of interest to develop a virtual variable guide vane system in which variable stagger is replaced by actuation on the blades themselves. This actuation is required to control the flow direction as the engine moves offdesign and the blades experience increasing levels of incidence. As incidence increases, the flow will tend to separate from the suction surfaces of the airfoils. This separation must be reduced or eliminated, so as to minimize the blockage it creates. Flow control has been explored extensively for the purpose of separation control, both for external and internal flows, and so is explored here for this purpose. It should be noted that, in such a virtual variable guide vane system, the problem of setting the stator exit flow angle remains. Possible fluidic solutions include the application of flow control to the suction surfaces of the rotors as well as the stators; and the application of turning control to the stators in addition to the separation control discussed in this paper.

Another application of flow control in compressors is on highly loaded blades that would separate under design conditions without control. The increased loading that flow control allows the blades to be designed with means that fewer blades are needed for the same turning or that increased turning is achieved for the same number of blades. Both translate into a reduction in weight and part counts.

Flow control has been applied to axial compressors by a number of authors, including Culley et al. [1] and Kirtley et al. [2]. Both used streamwise blowing, reenergizing what appeared to be laminar boundary layers, by direct momentum addition. Bons et al. [3,4] and Volino [5] have used vortex-generator jets to control laminar separation on low-pressure turbine blades. Vortex-generator jets have been shown to create streamwise vortices in both turbulent [6,7] and laminar [8] boundary layers. These vortices reenergize the boundary layer by transporting high-momentum freestream fluid into the inner boundary layer and transporting low-momentum fluid from the inner boundary layer away from the wall. It is this use of freestream momentum to reenergize the boundary layer that allows for a lower level of injected momentum to achieve the same level of control as a streamwise jet [9]. Further mass flow reduction may be achieved by pulsing the jet. Pulsing at prescribed frequencies also allows natural frequencies within the flow to be excited and generates more mixing than is achievable with a steady jet due to the presence of a starting vortex with each pulse. This paper explores the application of vortex-generator jets to the control of a separating, turbulent boundary layer on a simulated compressor blade at high incidence.

A number of parameters are important to the effective operation of vortex-generator jets and, although recommendations do exist within the literature, these are not conclusive in many cases. Important parameters include the pitch and skew angles, defined in Fig. 1, the jet pulse frequency, and the jet velocity. Skewing the jet leads to weakening of one of the two counter-rotating streamwise vortices created downstream of a normal jet issuing into a crossflow, leaving a single strong vortex. Compton and Johnston [6] and Khan and Johnston [7] have shown this experimentally in a turbulent boundary layer with no pressure gradient. Postl et al. [10] suggest that the presence of an adverse pressure gradient can significantly effect this vortex formation, finding in their computational analysis that a strong adverse pressure gradient in fact prevented the formation of the single strong streamwise vortex. A single strong vortex has been found to be more effective at reattaching a separated boundary layer than two weaker corotating vortices behind a pitched jet with no skew [9] or a normal jet [8], due to more effective momentum transfer across the boundary layer.

The strength of the vortex formed by vortex-generator jets is influenced by the angle of skew. Increasing the skew angle from zero toward 90° reduces the streamwise component of the jet momentum and, therefore, its direct contribution to reenergizing the inner boundary layer. It, however, appears to increase the maximum level of streamwise vorticity measured downstream. Bons et al. [3,4], Johari and Rixon [11], Hansen and Bons [8], and Sondergaard et al. [12] used jets with 90° of skew. Barberopoulos and Garry [13], however, recommended 60°, a conclusion supported by the experimental work of Milanovic and Zaman [14], who showed that skewed jets issuing into a turbulent flow with no pressure gradient produce the maximum streamwise vorticity when skewed at between 45 and 60°. Khan and Johnston [7] came to the same conclusion, while Selby et al. [15] showed that jets with 60° of skew achieved the best pressure recovery when controlling a turbulent separation occurring in the presence of an adverse pressure gradient. Luedke et al. [9] recommended 45° for removing separated flow on a hump diffuser with a pressure distribution simulating the suction surface of a compressor blade, but this was the only nonzero skew angle tested.

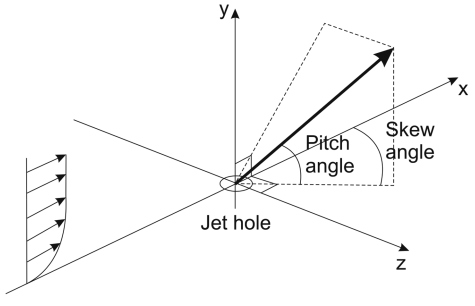

Fig. 1 Angle definitions for vortex-generator jets.

Barberopoulos and Garry [13] noted the sensitivity of the effect of this parameter to flow conditions and, therefore, the need to optimize skew angle for the application of interest.

The frequency of the jet pulses has received considerable attention within the literature, in many cases investigating the use of unsteady effects to increase lift [16,17]. Lift is augmented by the excitation of natural frequencies within the flow, such as the trailing-edge vortex shedding frequency or the shear layer instability [18]. In a compressor, however, a periodically separating and reattaching flow will introduce unacceptable unsteadiness into the wake that will propagate through and affect the performance of following blade rows, as well as increase the potential for high-cycle fatigue. Any natural frequency excitation that produces periodic separation and reattachment is, therefore, essentially ruled out of this application.

The mass flow reduction and increased mixing that pulsing makes possible are, however, still motivations to pursue pulsed blowing in this application. McManus et al. [19] have used pulsed vortex-generator jets to control a turbulent separation in a diffuser, concluding that pulsing can reduce the injected mass flow rate over steady blowing for the same level of control. There is still, however, a question as to the optimal frequency for the prevention of an open type of turbulent separation, such as occurs on a compressor blade at high incidence.

The jet velocity, or amplitude in the case of pulsed blowing, has also received much attention in the literature. Sondergaard et al. [12] found that the minimum loss coefficient for a low-pressure turbine blade controlled with steady vortex-generator jets occurred for a velocity ratio of around 1.0, where the jet velocity was normalized by the local freestream velocity. For higher velocities, no further loss reduction was observed. Nishri and Wygnanski [20] observed a hysteresis in the amplitude of a pulsed jet required to reattach a separated flow and in that required to subsequently keep the reattached flow from separating. In the application of a compressor, separation must be prevented as incidence increases, rather than controlled after it occurs. The hysteresis observed by Nishri and Wygnanski therefore highlights the need to ensure that the control investigated is preventing separation rather than reattaching an already separated flow.

The jet velocity is closely tied to the size of the jet hole, as the injected mass flow rate can be reduced for the same jet momentum by increasing the jet velocity and decreasing the hole size. This is the motivation behind the micro jets used by Kumar and Alvi [21], which are supersonic. For their application in a compressor, the pressure required to drive supersonic microjets will, however, be expensive, as it will have to be bled from high stages in the compressor. In this work, the jet velocity is therefore limited to subsonic values.

The lack of conclusive recommendations in the literature for the parameters listed suggested that a parametric study was necessary for the application of vortex-generator jets to keep the flow from separating at the trailing edge of a compressor blade at high incidence. It is this study that is discussed in the remainder of this paper. Three parameters are explored: jet velocity, jet skew angle, and actuation frequency.

II. Experimental Facilities and Procedures

The parametric study was performed in a flat-plate rig located at the exit of a low-speed continuous blower-type wind tunnel at the Whittle Laboratory. The flat-plate rig is shown schematically in Fig. 2. The flat plate was placed between contoured endwalls that set up identical velocity distributions on the top and bottom surfaces of the plate. These create the pressure distribution of the suction surface of a compressor blade provided by MTU Aero Engines (MTU). The pressure distribution on the flat plate simulates the compressor blade suction surface at 12.5° of incidence. The pressure distribution is defined such that the blade trailing edge coincides with an effective trailing edge on the flat plate at a surface distance of 486 mm from the leading edge. This effective trailing edge allows an effective chord of 463 mm to be calculated from the ratio of chord to suction surface length on the MTU blade. The effective trailing edge is shown in Fig. 2. The flat plate is 765 mm long and has a span of 460 mm.

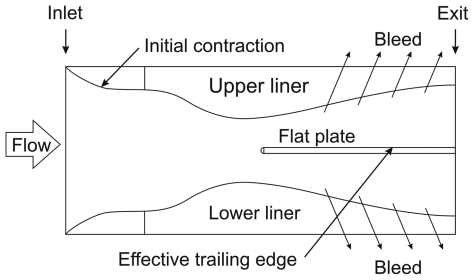

Fig. 2 Schematic of flat-plate rig.

Bleed through the endwalls and sidewalls prevents separation on these surfaces, forcing it to occur on the flat plate itself. The bleed on these surfaces was set by opening holes in the surfaces to remove any separated flow on them. The flow on the liners and sidewalls was interrogated using tuft flow visualization to confirm the absence of flow separations. The bleed on these surfaces was held constant for all cases tested. The flat plate extends to the exit of the wind tunnel, where a mesh screen is located. The screen suppresses any vortex shedding off the trailing edge of the flat plate and pressurizes the test section to above ambient pressure. This allows bleed to be achieved without suction, with the bleed holes and slots in the endwalls and sidewalls connected to the atmosphere. The mesh screen was chosen to ensure that a high enough pressure was achieved inside the rig to ensure that the endwall and sidewall bleeds were, in fact, bleeds and not injections in all operating cases.

The jet holes are built into circular plugs on the upper surface of the flat plate. The rotation of these plugs allows the skew angle to be varied over a range from 45 to 90°. Each plug is supplied with air through an array of plastic tubes inside the flat plate. A siren valve is used to generate a variety of pulsed jet signals on the surface of the flat plate. Laboratory air is supplied to the siren valve from which it is sent to the individual jet holes via a manifold, which is approximately 630 cm^3 in volume. The resonant frequencies of the system are in the order of 15 Hz and the harmonics thereof. Each jet hole is built into one plug. An example is shown sitting on top of the plate in Fig. 3. The jet holes are 4.5 mm in diameter, which is 0.18 of the local boundary-layer thickness and 0.55 of the local displacement thickness. These ratios are similar to the holes used by Bons et al. [3,4] and Volino [5]. The jet holes are spaced by 53 mm (i.e., 11.8 diameters). This distance was limited by the design of the jet injection system, but it is close to the 12 diameters recommended by Yip [22]. A hot-wire anemometer was placed at the exit of one jet hole so that the pulsed jet velocity signal could be measured directly. Examples of measured velocity signals are shown in Fig. 4 for frequencies of 100 and 600 Hz. These frequencies correspond to reduced frequencies F^+ of 0.9 and 5.5, respectively. The reduced frequency F^+ is defined in Eq. (1) as a function of the inlet flow velocity V_1 and the length L of the separation region on the flat-plate surface in the baseline unactuated case. The length L is 145 mm, which is 31% of the effective chord. The two signals are shown over the same time period. Three pulses are shown for the 100 Hz signal, and 18 pulses are shown for the 600 Hz signal. Both at 100 and 600 Hz, the pulses have reasonably steep leading and trailing edges and approach zero velocity between pulses. This signal shape is similar to that produced by a microelectromechanical-systems device developed for actuation in a real engine [23]:

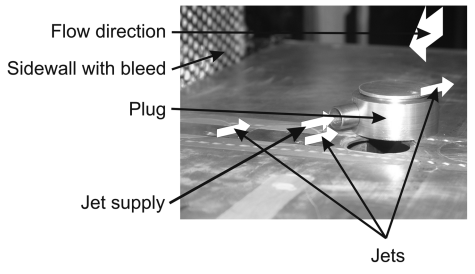

Fig. 3 Jet-hole plug on surface of flat plate.

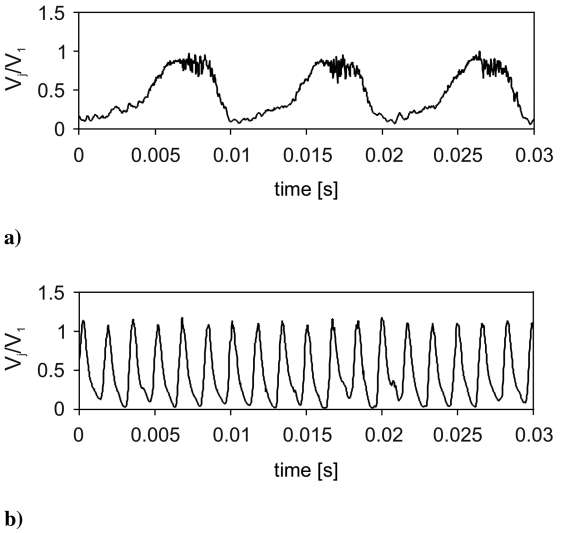

Fig. 4 Jet velocity signal generated by siren valve at a) 100 and b) 600 Hz.

$$F^+ = \frac{fL}{V_1} \tag{1}$$

The pressure distribution on the flat plate was measured by means of static pressure tappings located along the length of the plate, 10% of span offset from the centerline. The last pressure tapping coincides with the effective trailing edge of the flat plate. Stagnation pressure was measured by means of a pitot probe, traversed at this effective trailing edge over an area one jet-hole pitch in span and 130 mm in the direction normal to the flat-plate surface. This normal dimension is larger than the boundary layer measured in all cases tested.

Flow control is only applied to the upper surface of the flat plate. In the cases in which this control removes the separation occurring on this surface, the blockage in the upper flow passage is reduced, while that in the lower flow passage remains the same. The symmetry of the flat plate is thus lost in these cases. The asymmetry in blockage would suggest that the mass flow rate through the upper passage increases and that through the lower passage decreases. Static pressure measurements made on the upper surface of the flat plate did not, however, show any increase in velocity over the forward part of the flat plate, suggesting that this effect is small.

The metric used to evaluate the effectiveness of flow control for the various configurations tested is the mixed-out stagnation-to-stagnation pressure loss coefficient. The loss coefficient is defined in Eq. (2) for an equivalent cascade blade. This loss coefficient includes the stagnation-to-stagnation pressure profile loss coefficient Y_p normalized by inlet conditions, as well as the loss coefficient generated by the mixing of the injected jet fluid with the mainstream fluid Y_j. These terms are defined in Eqs. (3) and (4), respectively:

$$Y = Y_p + \left(\frac{\dot{m}_j}{\dot{m}_1}\right) Y_j \tag{2}$$

$$Y_p = \frac{p_{01} - p_{02}}{\frac{1}{2}\rho V_1^2} \tag{3}$$

$$Y_j = \frac{p_{0j} - p_{02}}{\frac{1}{2}\rho V_1^2} \tag{4}$$

With Eq. 5, the measurements taken on the flat plate were used to calculate the mixed-out profile loss coefficient defined in Eq. (3). Equation (5) shows the loss coefficient as a function of the displacement thickness δ^* and the momentum thickness θ on the trailing edge of the equivalent cascade blade:

$$Y_p = \left(\frac{V_2}{V_1}\right)^2 \Bigg[\underbrace{\left(\frac{s\cos\alpha_2}{s\cos\alpha_2 - t - \delta^*}\right)^2 \frac{2\theta}{s\cos\alpha_2}}_{\text{boundary-layer term}} + \underbrace{\left(\frac{\delta^* + t}{s\cos\alpha_2 - t - \delta^*}\right)^2}_{\text{blockage term}} \Bigg] \tag{5}$$

Equation (5) is based on an equation for the loss coefficient derived as a function of δ^* and θ by Denton [24]. The complete derivation of Eq. (5) can be found in Appendix A of Evans [25]. The bleed flows through the endwalls and sidewalls of the flat-plate experimental facility are not included in the loss formulation, because the loss coefficient represents the profile loss of an equivalent cascade blade. The inlet mass flow rate $\dot{m}_1$ used in Eq. (2) is defined for an area made by the equivalent blade pitch s and the pitch between two jet holes. The jet mass flow rate $\dot{m}_j$ is then the mass flow rate through one jet hole. The jet stagnation pressure p_{0j} was measured in the jet supply tubing, just upstream of the jet-hole plug assembly, supplying one jet hole.

Equation (5) consists of two terms: a boundary-layer term based on the momentum thickness θ at the effective trailing edge and a blockage term based on the displacement thickness δ^* at the effective trailing edge. The base pressure term has been omitted, since there is no trailing edge on the flat plate, and the variation of this term with control is not known. This term is likely to be small in this application. The trailing-edge thickness t and effective blade pitch s are scaled from the MTU blade from which the pressure distribution on the flat plate comes. The effective blade pitch is 303 mm. The equivalent exit flow angle for the baseline unactuated case was calculated from the inlet flow angle of the MTU blade, using Eq. (6):

$$\Gamma = sV_x(\tan\alpha_1 - \tan\alpha_2) \tag{6}$$

The circulation in this equation was estimated using the measured velocity distribution on the flat plate, to represent the suction surface velocity distribution, and the pressure surface velocity distribution computed on the pressure side of the MTU blade using the MISES computational fluid dynamics (CFD) code. This is a two-dimensional (2-D) Euler code coupled with an integral boundary-layer solver. The axial velocity V_x was taken as the cosine of the calculated exit flow angle multiplied by the exit velocity measured in the baseline experiment.

For all actuated cases, the exit flow angle was adjusted according to the change in circulation calculated from the measured velocity distribution on the surface of the flat plate. The pressure side contribution was assumed to remain constant.

The displacement thickness and momentum thickness were calculated from the area traverse measurements of the stagnation pressure taken at the effective trailing edge. The static pressure was assumed to be equal to the surface static pressure at the effective trailing edge, measured by means of the static pressure tapping at this axial location.

The ratio of the jet velocity to either inlet or local freestream velocity is typically used in the literature to nondimensionalize the jet velocity. The injected momentum coefficient is also used, and it is recommended by Luedke et al. [9] as the correct parameter to scale the hole diameter for cases in which the jet holes are spaced by more than 6 diameters. The injected momentum coefficient is defined as the injected momentum flux divided by the product of the inlet dynamic head and some area, usually the product of the span and a length scale that is not consistent across the literature. The length scales used include the length of the separation region [1,20], the airfoil chord [2,9,16], and the inlet boundary-layer thickness [21]. Since the purpose here is to explore the application of flow control in a compressor, the blade pitch multiplied by the cosine of the inlet flow angle was used. This yields an injected momentum coefficient that is proportional to the ratio of the jet to the inlet momentum flux. This is a meaningful definition of the injected momentum coefficient in this application. The injected momentum coefficient C_μ is thus defined, in Eqs. (7–9), in terms of the exit area of one jet A_j, the number of jets on the flat plate n, and the plate span b:

$$C_\mu = \bar{C}_\mu + C'_\mu \tag{7}$$

The time-mean component is defined in Eq. (8):

$$\bar{C}_\mu = \frac{2nA_j}{bs\cos(\alpha_1)}\left(\frac{\bar{V}_j}{V_1}\right)^2 \tag{8}$$

The harmonic oscillation component is defined in Eq. (9):

$$C'_\mu = \frac{2nA_j}{bs\cos(\alpha_1)}\left(\frac{\sqrt{V'^2_j}}{V_1}\right)^2 \tag{9}$$

III. Experimental Results

A. Baseline Performance

The bleed through the sidewalls, necessary to prevent these surfaces from separating, introduced spanwise flow over the edges of the flat-plate span. The central 60% of the span, however, had a straight separation line extending across it in the spanwise direction. The Reynolds number, based on the effective chord, was 500,000, which is typical of an early-stage intermediate-pressure compressor blade. A laminar separation bubble with turbulent reattachment was observed close to the leading edge of the flat plate, using oil flow visualization. The boundary layer was therefore known to be turbulent over the majority of the flat-plate surface.

Under baseline unactuated flow conditions the velocity distribution calculated from measured static pressures indicates that the flat-plate boundary layer separated at 70% surface distance normalized by surface distance to the effective trailing edge. This velocity distribution is shown in Fig. 5. Since the boundary layer was known to be turbulent at this point, this is a turbulent boundary-layer separation. The jets were located at 62% surface distance, 8% surface distance upstream of separation. This location was based on the observed separation location, geometric constraints within the flat plate, and the recommendations of Gad-el-Hak [26] and Bons et al. [4] to place the actuator as close to separation as possible. The freestream velocity at the jet location was 0.82 of the inlet flow velocity. The measured separation location was upstream of the separation location predicted by the MISES 2-D CFD code when run on the MTU blade. MISES predicted separation at 78% suction surface length. The difference is believed to be due to a combination of the presence of the screen downstream of the separation in the case of the flat-plate experiment and the leading edge on the flat plate. The laminar separation bubble observed near the leading edge of the flat plate was not observed in the MISES calculation of the blade.

The displacement thickness measured at the effective trailing edge in the baseline unactuated case was 63 mm. The momentum thickness was 7.4 mm. The mixed-out stagnation-to-stagnation pressure loss coefficient was calculated, using Eq. (5), and averaged over one jet-hole pitch as 0.095 ± 0.004.

B. Influence of Injected Momentum Coefficient

Steady injection was performed with a jet skew angle of 60° and a steady jet velocity ranging from $0.8V_1$ to $1.5V_1$. The injected

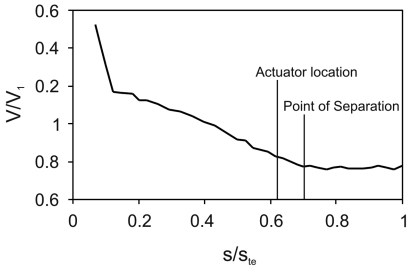

Fig. 5 Velocity distribution on the surface of the flat plate for the baseline unactuated flow.

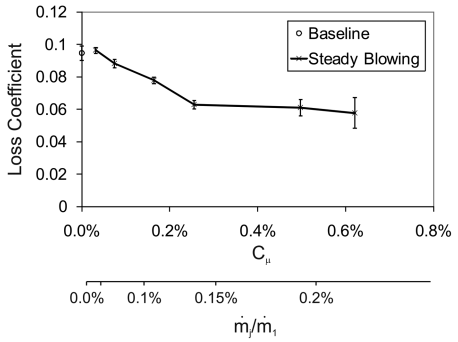

Fig. 6 Influence of injected momentum coefficient on loss coefficient for steady blowing. Ratio of injected-to-inlet mass flow rate also shown.

momentum coefficient is plotted against the mixed-out loss coefficient in Fig. 6. The ratio of the injected to inlet mass flow rate is also shown. The variation in the injected momentum coefficient was achieved by varying the jet velocity while holding the hole diameter constant. As with the baseline unactuated data, the loss coefficient is averaged over one jet-hole pitch. Also shown in Fig. 6 is the loss coefficient for the baseline unactuated case in which the injected momentum coefficient is zero.

Figure 6 shows that steady blowing reduced the loss coefficient relative to the baseline for all jet velocities tested, the loss coefficient decreasing with increasing injected momentum until a threshold was reached beyond which no significant further loss reduction was achieved. This threshold occurs at an injected momentum coefficient of 0.26%, which corresponds to a jet velocity approximately equal to V_1 and an injected mass flow rate equal to 0.13% of the inlet mass flow rate. This is 1.2 times the local freestream velocity. This result is similar to the results of Sondergaard et al. [12], who found that the loss reduction achieved with vortex-generator jets in a laminar flow on a low-pressure turbine blade increased with increasing jet velocity, up to a jet velocity of 1.5 times the local freestream velocity. Higher jet velocities yielded no further loss reduction. The mechanism by which control was achieved in the work reported in Sondergaard et al. [12] is, however, believed to be the promotion of transition rather than the generation of a streamwise vortex. Since the boundary layer studied in the present case is turbulent, the mechanism by which control is achieved is believed to be the generation of a vortex.

Figure 7 shows the loss coefficient plotted in Fig. 6 broken into the two terms described in Eq. (2), the first of which is further broken into the two terms described in Eq. (5). The figure shows the three terms stacked on top of one another, so that the upper line is the total loss coefficient shown in Fig. 6. The jet term [the second in Eq. (2)] is shown to be small, relative to the two terms making up the profile loss coefficient Y_p, and it increases with increasing injected momentum. The two terms making up the profile loss coefficient are of similar magnitude, and both decrease with increasing injected momentum. Figure 7 shows that the loss reduction shown in Fig. 6 is primarily driven by the blockage term in Eq. (5), which is a function of the displacement thickness. The boundary-layer term, which is a function of the momentum deficit caused by the presence of the boundary layer, also drops with increasing injected momentum coefficient but contributes less to the overall reduction in the loss coefficient.

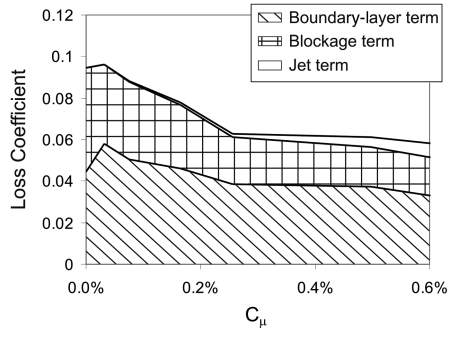

Fig. 7 Influence of injected momentum coefficient on the components of loss coefficient for steady blowing.

Velocity contours derived from the stagnation pressure measurements taken at the effective trailing edge are shown in Fig. 8 for four different jet velocities. The span shown is one jet-hole pitch. Comparing contours at low-jet velocities, shown in Figs. 8a and 8b, it is evident that the boundary layer thinned as the jet velocity, and hence the injected momentum coefficient, was increased. The contours for blowing at a jet velocity equal to $1.0V_1$ ($C_\mu = 0.26\%$) show a thinner boundary layer than at a jet velocity equal to $0.8V_1$ ($C_\mu = 0.16\%$). These contours show little variation in the spanwise direction, except for a slightly thinned boundary layer to the left of the jet hole for a jet velocity equal to $1.0V_1$. The slight departure from periodicity in the spanwise direction is a result of the crossflow introduced into the flow passage by all jets being skewed in the same direction, which disturbed the balance in bleed imposed on the sidewalls.

For the cases with jet velocities equal to $1.3V_1$ ($C_\mu = 0.5\%$) and $1.5V_1$ ($C_\mu = 0.62\%$), shown in Figs. 8c and 8d, the thickness of the boundary layer is shown to vary in the spanwise direction to a greater degree than the cases shown in Figs. 8a and 8b. The boundary layer was thinned to a greater degree in these cases than in the case with a jet velocity equal to $1.0V_1$, and it was thinned over only part of the span traversed. This spanwise variation in boundary-layer thickness was a result of the streamwise vortex created by the jets. The effect of this vortex in turning high-momentum fluid from the outer to inner boundary layer is more clearly evident for these higher velocities, although the vortex is believed to be responsible for the thinned boundary layer to the left of the jet hole, evident in Fig. 8b, for a jet velocity equal to V_1.

Although the spanwise extent of the thinned boundary layer between jet holes was the same at the two higher jet velocities, the spanwise position varied. For a jet velocity equal to $1.3V_1$, shown in Fig. 8c, the thinned boundary layer extended from 20% of the hole

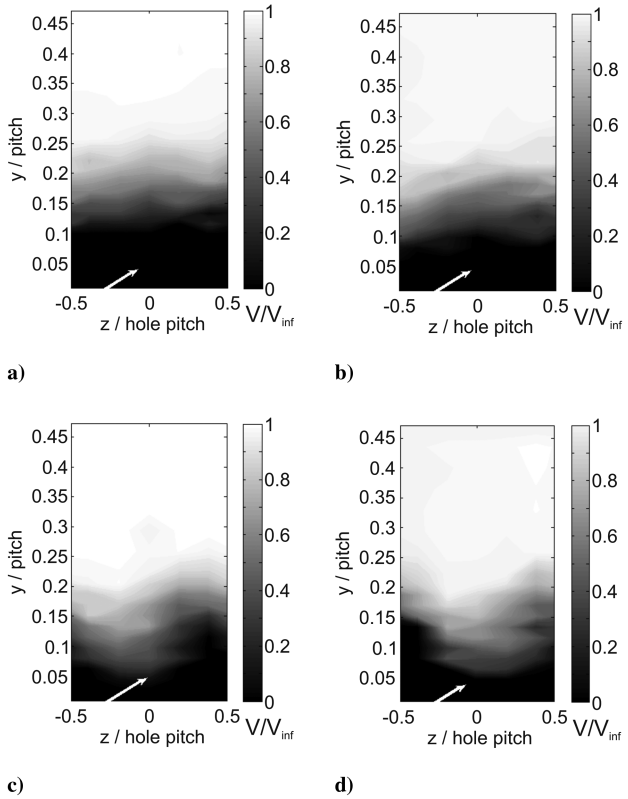

Fig. 8 Contours of time-averaged velocity normalized by freestream velocity. Measured at the effective trailing edge of the flat plate for steady blowing at a) $V_j = 0.8V_1$, b) $V_j = V_1$, c) $V_j = 1.3V_1$, and d) $V_j = 1.5V_1$. Jets shown with white arrows.

pitch to the left of the jet hole to 40% of the hole pitch to the right of the jet hole. For a jet velocity equal to $1.5V_1$, shown in Fig. 8d, however, the thinned boundary layer extended from the jet hole to 60% of the hole pitch to the right of the jet hole. This movement of the thinned portion of the boundary layer was a result of the increased spanwise component of the jet velocity in the $1.5V_1$ jet velocity case, which pushed the streamwise vortex created by the jet further to the right than in the $1.3V_1$ jet velocity case.

The spanwise average effect is an approximately constant boundary-layer thickness for jet velocities above V_1. The spanwise shape of these velocity contours is consistent with other experimental results, including those of Compton and Johnston [6] and Honami et al. [27], who used 90°-skewed jets blowing at velocity ratios between 0.6 and 1.4 in a turbulent boundary layer with zero pressure gradient. The shape is also consistent with the results of Khan and Johnston [7], who used 60°-skewed jets blowing at a velocity ratio of 1.0 into a turbulent boundary layer with zero pressure gradient. These contours confirm the presence of a single streamwise vortex created by the vortex-generator jets in a turbulent flow and in the presence of an adverse pressure gradient.

C. Influence of Jet Skew Angle

Figure 9 shows the influence of the jet skew angle on the loss coefficient for steady blowing. The skew angle was set at three angles: 45, 60, and 90°. Figure 9 shows that the 90°-skewed jets generated a loss increase for an injected momentum coefficient below 0.26%. Above this injected momentum coefficient, however, the 90°-skewed jets did reduce the loss coefficient over the baseline unactuated case. Both 45 and 60°-skewed jets are shown to be more effective at reducing the loss coefficient over the whole range of injected momentum coefficient tested. This is likely to be attributable to the component of jet velocity in the streamwise direction, adding momentum directly to the boundary layer. At low-injected momentum, when the streamwise vortex is weak, this streamwise velocity component is important in directly adding momentum to the boundary layer. As the jet velocity increases, however, and the strength of the streamwise vortex increases, this streamwise velocity component becomes less important in reenergizing the boundary layer relative to the increasing momentum drawn into the inner boundary layer from the mainstream by the streamwise vortex. This explains why the data for the 90°-skewed jet are able to approach that for the 45 and 60°-skewed jets at higher injected momentum coefficients.

Injection at skew angles of 45 and 60° generated a similar loss reduction at high-injected momentum coefficients, corresponding to high-jet velocity. At low-injected momentum coefficients, however, the 60°-skewed jets generated a greater loss reduction. A balance must be reached between the strength of the vortex created, which increases with skew angle, and the velocity component in the streamwise direction, which decreases with skew angle. Of the angles tested, a skew angle of 60° appears to be the best at low-injected momentum coefficient.

D. Influence of Actuation Frequency

Pulsed blowing was performed over a range of frequency from 50 to 780 Hz. This is equivalent to a range of reduced frequency from 0.5 to 7.1. The mixed-out stagnation-to-stagnation pressure loss coefficient is presented in Fig. 10 as a function of the reduced frequency and the injected momentum coefficient. The loss data were time-averaged over 2 s. Figure 10 also shows the data for the baseline unactuated case and that for steady blowing. The data for pulsed blowing, shown in Fig. 10, were produced with varying levels of peak jet velocity, ranging from $0.8V_1$ to $1.5V_1$. The same range of jet velocity was used as in the steady blowing experiments. Between pulses, the jet velocity approached zero, as shown in the example jet velocity traces in Fig. 4. At all frequencies plotted, the duty cycle was approximately 60%, and the signal shape was approximately constant. Figure 10 shows pulsed blowing data at only four reduced frequencies. More were generated, but they have been left off the figure for the sake of clarity.

The point of the maximum injected momentum coefficient shown on each line in Fig. 10 is for a peak jet velocity of $1.5V_1$. The reduction in injected momentum due to pulsing is evident in Fig. 10 when comparing the pulsed data with the steady data. For pulsed blowing with jet signals of similar shape, the injected momentum coefficient was a function of the duty cycle only. The duty cycle was held approximately constant for all the pulsed data plotted, making the injected momentum coefficient at a peak jet velocity of $1.5V_1$ approximately constant.

Figure 10 shows that pulsed blowing reduced the loss coefficient over the baseline unactuated case for all frequencies tested. At and below a reduced frequency of 3.5, the loss relative to the baseline was, however, greater than was achieved with steady blowing at the same injected momentum coefficient. Only at a reduced frequency of 5.5 was the loss achieved by pulsed blowing lower than that achieved with steady blowing at the same injected momentum coefficient. This can be seen more clearly in Fig. 11, in which the loss coefficient is plotted against the reduced frequency for lines of constant injected momentum coefficient. Also shown in Fig. 11 is the loss coefficient for steady blowing at the same injected momentum coefficient as for the pulsed blowing data. The loss coefficient for the baseline unactuated case is also shown. Figure 11 shows that the loss increased slightly with increasing reduced frequency up to a reduced frequency of 1.4, beyond which the loss decreased with increasing reduced frequency. The loss coefficient remained reasonably constant above a reduced frequency of 4.5. The loss reduction was equal to that achieved with steady blowing at the same injected momentum coefficient at a reduced frequency of 4.8 for both $C_\mu = 0.2\%$ and $C_\mu = 0.1\%$. The higher-momentum jet ($C_\mu = 0.2\%$) generated a lower loss coefficient than the steady jet for a reduced frequency above 4.8. The minimum loss coefficient measured was 4% lower than that achieved with the steady jet of the same injected momentum coefficient. The lower-momentum jet ($C_\mu = 0.1\%$) achieved a minimum loss coefficient 3% lower than that achieved with the steady jet of the same injected momentum coefficient.

Figure 12 shows the loss coefficient plotted against the reduced frequency for lines of constant peak jet velocity. In an early stage of an intermediate-pressure compressor, with an stage inlet flow Mach number of 0.75, the velocity in a subsonic jet is limited to approximately $1.3V_1$. It is therefore interesting to consider the data plotted for lines of constant peak jet velocity.

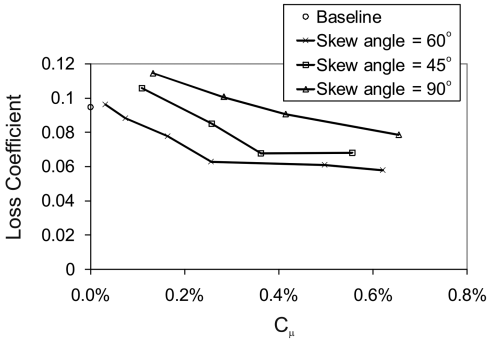

Fig. 9 Influence of jet skew angle on loss coefficient for steady blowing.

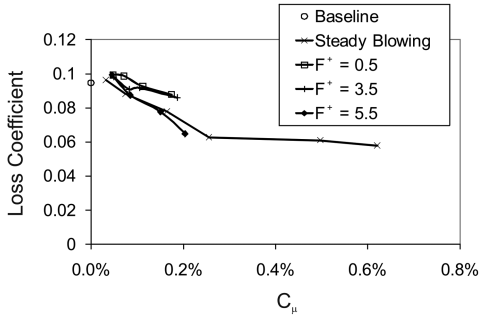

Fig. 10 Influence of jet frequency and injected momentum coefficient on loss.

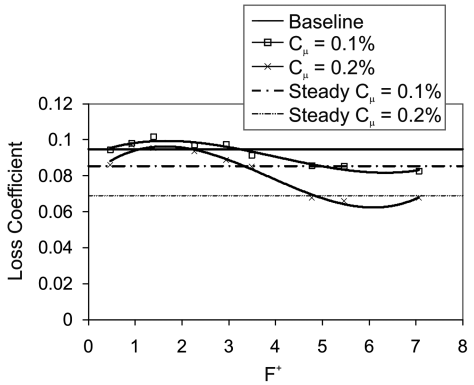

Fig. 11 Loss versus reduced frequency for lines of constant injected momentum coefficient.

As in Fig. 11, the loss coefficient for steady blowing at the same jet velocity as the peak jet velocity of the pulsed blowing data is also shown in Fig. 12. As expected, Fig. 12 shows similar trends to those shown in Fig. 11. At all peak jet velocities tested, the loss coefficient is shown to have decreased to a minimum at the highest reduced frequency tested (i.e., seven). However, only the pulsed jet with a peak jet velocity equal to $1.5V_1$ generated the same loss coefficient as the steady jet with the same jet velocity at this minimum. The lines for lower peak jet velocities are shown not to have reached as low a loss coefficient as achieved with steady blowing with the same jet velocity in the range of reduced frequency tested.

For the same loss reduction, pulsed blowing with a peak jet velocity of $1.5V_1$ yielded a reduction in the jet mass flow rate of 40%, relative to the best steady blowing case. However, with the peak jet velocity limited to $1.3V_1$ in a real engine, these results suggest that, within the range of reduced frequency tested, pulsed blowing with a subsonic jet is not able to generate the same loss reduction as the best steady blowing case. Higher reduced frequencies may, however, yield further loss reduction for the lower peak jet velocity cases, enabling a subsonic jet to achieve the same loss reduction as the best steady jet.

Time-averaged trailing-edge velocity contours are shown for pulsed blowing at reduced frequencies of 0.9 and 5.5 in Figs. 13 and 14 respectively. Considering Fig. 13, which shows contours of velocity for 4 cases of increasing peak jet velocity, it is clear that pulsed blowing at a reduced frequency of 0.9 had little influence in the time-averaged trailing-edge velocity contours at any of the jet velocities tested. At the higher frequency plotted in Fig. 14; however, the time-averaged boundary layer was thinned by the increasing peak jet velocity. Comparing the trailing-edge velocity contours for high-frequency pulsed blowing, shown in Fig. 14, with the contours for steady blowing, shown in Fig. 8, it is clear that the level of spanwise variation was lower in the pulsed case than in the steady case. This is likely to be either an effect of the time-averaging or increased mixing resulting from the presence of starting vortices with each pulse.

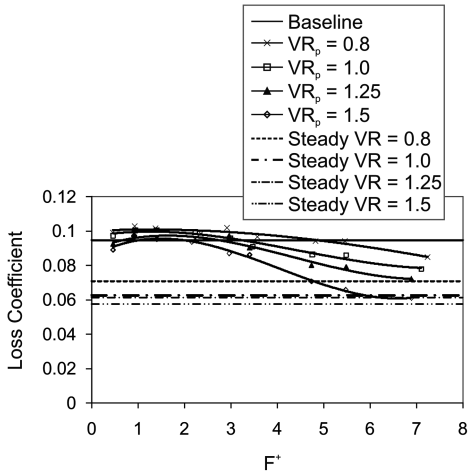

Fig. 12 Loss coefficient versus reduced frequency for lines of constant peak jet velocity ratio, VR_p. Steady blowing also shown at the same velocity ratio (VR).

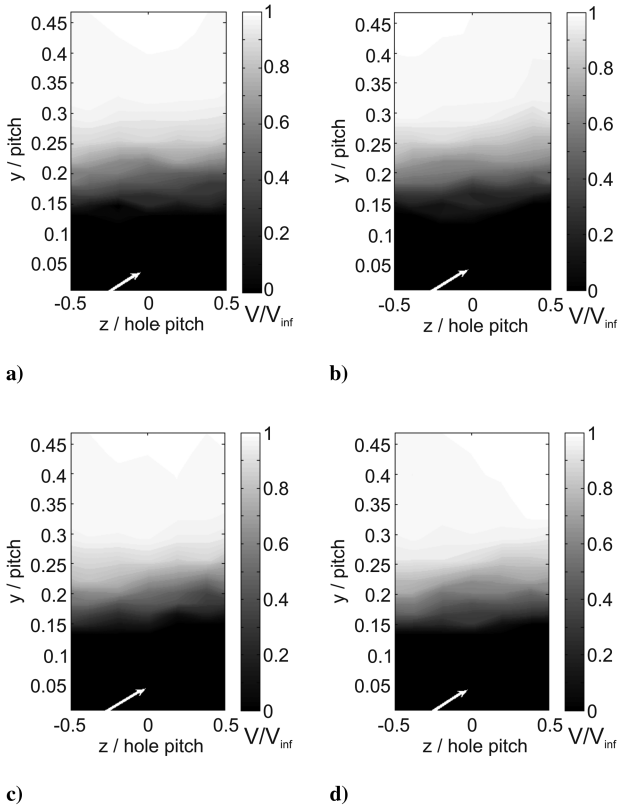

Fig. 13 Contours of time-averaged velocity normalized by freestream velocity. Measured at the effective trailing edge of the flat plate for pulsed blowing at $F^+ = 0.9$ at a) $V_j = 0.8V_1$, b) $V_j = V_1$, c) $V_j = 1.3V_1$, and d) $V_j = 1.5V_1$.

Pulsed blowing has been found to be most effective when exciting a natural frequency in the flow. An open separation that does not reattach before the trailing edge is subject to two natural frequencies: the wake shedding frequency and the natural frequency of the shear layer instability. The flow over the flat plate does not shed off the trailing edge due to the presence of the mesh screen and is, therefore, not subject to a shedding frequency. The presence of a shear layer instability is, however, quite possible. It is, however, difficult to estimate the frequency of this instability, as it is a function of the turbulent separation occurring at 70% surface distance, the turbulent boundary layer upstream of it, and the laminar separation bubble that exists close to the leading edge of the flat plate. The improved effectiveness of pulsed actuation at higher frequencies over a lower frequency may be due to excitation at frequencies to which the shear-layer instability is responsive.

The loss results presented previously suggest that, although pulsed blowing can be as effective at reducing the loss coefficient as steady blowing, a high-pulse frequency and high-jet velocity are required. A reduced pulse frequency of at least 6.0 was required to match the loss reduction of steady blowing, and this was accompanied by peak jet velocities equal to 1.5 times the inlet flow velocity. This is compared with steady blowing jet velocities equal to the inlet flow velocity. In a real intermediate-pressure compressor, these numbers translate into pulsed jets with a peak Mach number of 1.125, pulsing at more than 180 kHz, and steady jets with a Mach number of 0.75. Even high-subsonic pulsed jets would need to be supplied from a higher pressure than the steady jets to generate the same loss reduction, although they would save 40% of jet mass flow rate.

To achieve a frequency of 180 kHz in a full-size compressor, with the jet velocity approaching zero between pulses (and even high-subsonic Mach numbers during pulses) actuation would need to be

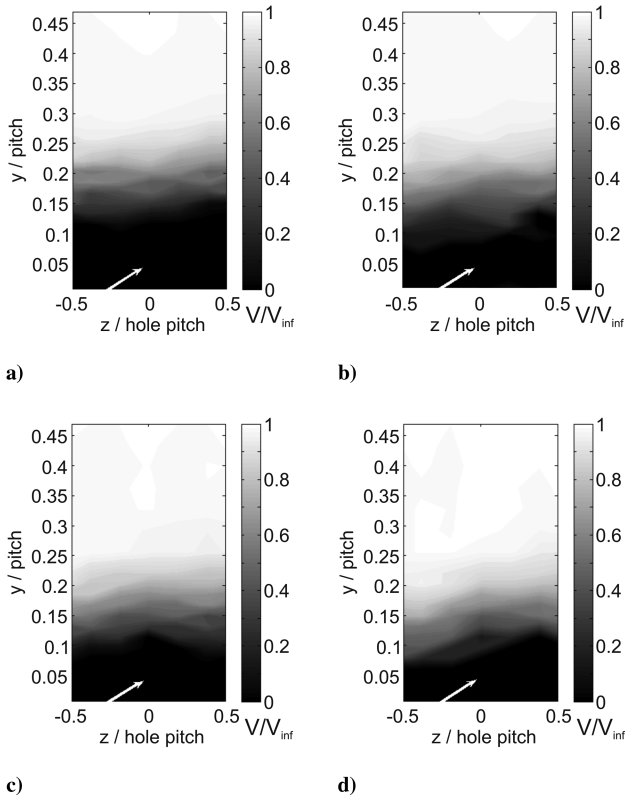

Fig. 14 Contours of time-averaged velocity normalized by freestream velocity. Measured at the effective trailing edge of the flat plate for pulsed blowing at $F^+ = 5.5$ at a) $V_j = 0.8V_1$, b) $V_j = V_1$, c) $V_j = 1.3V_1$, and d) $V_j = 1.5V_1$. $= 1.5V_1$..

performed on the blade surface. Any ducting between the actuator and the jet hole would introduce inertia into the jet flow, which would dampen the pulse signal and make the jet velocities harder to achieve. A full-size blade with an aspect ratio of 3.5 and a chord of 50 mm would need 30 jets spaced by 5.5 mm, with 0.5 mm diameter jet holes. Since these blades are likely to have a maximum thickness of just 3.5 mm, placing the actuation on the surface presents a significant structural challenge. The complexity of the system, supplied with air bled from downstream in the compressor, is significant.

Using the results presented previously to recommend the use of steady or pulsed blowing on a compressor blade must, however, be performed with caution. The flat-plate experimental facility is a model of a compressor blade that does not include important real effects, such as upstream wakes, neighboring blades, and changes in blade circulation, among others. It is due to this latter limitation that flow turning has not been considered as a metric of performance. To more fully evaluate the viability of flow control by steady or pulsed blowing in a compressor, flow turning must be considered along with the loss coefficient.

IV. Conclusions

Vortex-generator jets have been used for the control of a turbulent open separation in a diffusing flow, simulating that on the suction surface of a compressor blade. A parametric study has been carried out in which the injected momentum coefficient, pulse frequency, and jet skew angle were varied. A maximum loss reduction of 36% was achieved when compared with the baseline unactuated case. This was achieved with steady blowing, with an injected momentum coefficient of 0.26% and a skew angle of 60°. This corresponds to an injected mass flow rate of 0.13% of the inlet mass flow rate and to a jet Mach number of 0.75 in an early stage of a full-size intermediate-pressure compressor. Increasing the injected momentum coefficient beyond 0.26% did not achieve further loss reduction over the baseline unactuated case.

Pulsing the jets with a duty cycle of 60% allowed for a reduction in the jet mass flow rate of 40% but required a higher peak jet velocity to achieve the same loss reduction as that achieved with steady blowing. High-frequency actuation was needed, with a reduced frequency greater than 6.0. This corresponds to more than 180 kHz and jets blowing at Mach 1.125 in an early stage of a full-size intermediate-pressure compressor. Low-frequency pulsing was not found to be very effective at reducing the loss coefficient.

Acknowledgments

This project is supported by funding under the Sixth Research Framework Program of the European Union, Project ADVACT (Advanced Actuation Concepts), contract no. 502844. The excellent standards and support of the technical staff at the Whittle Laboratory are also acknowledged.

References

[1] Culley, D. E., Bright, M. M., Prahst, P. S., and Strazisar, A. J., "Active Flow Separation Control of a Stator Vane Using Surface Injection in a Multistage Compressor Experiment," *Proceedings of ASME Turbo Exposition*, American Society of Mechanical Engineers, GT2003-38863, New York, 2003.

[2] Kirtley, K. R., Graziosi, P., Wood, P., Beacher, B., and Shin, H.-W., "Design and Test of an Ultra-Low Solidity Flow-Controlled Compressor Stator," *Proceedings of ASME Turbo Exposition*, American Society of Mechanical Engineers, GT2004-53012, New York, 2004.

[3] Bons, J. P., Sondergaard, R., and Rivir, R. B., "The Fluid Dynamics of LPT Blade Separation Control Using Pulsed Jets," *Proceedings of ASME Turbo Exposition*, American Society of Mechanical Engineers, 2001-GT-0190, New York, 2001.

[4] Bons, J. P., Sondergaard, R., and Rivir, R. B., "Turbine Separation Control Using Pulsed Vortex Generator Jets," *Journal of Turbomachinery*, Vol. 123, No. 2, 2001, pp. 198–206. doi:10.1115/1.1350410

[5] Volino, R. J., "Separation Control on Low-Pressure Turbine Airfoils Using Synthetic Vortex Generator Jets," *Journal of Turbomachinery*, Vol. 125, No. 4, 2003, pp. 765–777. doi:10.1115/1.1626686

[6] Compton, D. A., and Johnston, J. P., "Streamwise Vortex Production by Pitched and Skewed Jets in a Turbulent Boundary Layer," *AIAA Journal*, Vol. 30, No. 3, March 1992, pp. 640–647. doi:10.2514/3.10967

[7] Khan, Z. U., and Johnston, J. P., "On Vortex Generating Jets," *International Journal of Heat and Fluid Flow*, Vol. 21, No. 5, 2000, pp. 506–511. doi:10.1016/S0142-727X(00)00038-2

[8] Hansen, L., and Bons, J. P., "Flow Measurements of Vortex Generator Jets in Separating Boundary Layer," *Journal of Propulsion and Power*, Vol. 22, No. 3, May–June 2006, pp. 558–566. doi:10.2514/1.13820

[9] Luedke, J., Graziosi, P., Kirtley, K., and Cerretelli, C., "Characterization of Steady Blowing for Flow Control in a Hump Diffuser," *AIAA Journal*, Vol. 43, No. 8, Aug. 2005, pp. 1644–1652. doi:10.2514/1.12797

[10] Postl, D., Gross, A., and Fasel, H. F., "Numerical Investigation of Low Pressure Turbine Blade Separation Control," 41st AIAA Aerospace Science Meeting and Exhibit, AIAA Paper 2002-614, Jan 2003.

[11] Johari, H., and Rixon, G. S., "Effects of Pulsing on a Vortex Generator Jet," *AIAA Journal*, Vol. 41, No. 12, Dec. 2003, pp. 2309–2315. doi:10.2514/2.6836

[12] Sondregaard, R., Rivir, R. B., and Bons, J. P., "Control of Low-Pressure Turbine Separation Using Vortex-Generator Jets," *Journal of Propulsion and Power*, Vol. 18, No. 4, July–Aug. 2002, pp. 889–895. doi:10.2514/2.6014

[13] Barberopoulos, A. A., and Garry, K. P., "The Effect of Skewing on the Vorticity Produced by an Airjet Vortex Generator," *The Aeronautical Journal*, Vol. 102, No. 1013, March 1998, pp. 171–177.

[14] Milanovic, I. M., and Zaman, K. B. M. Q., "Fluid Dynamics of Highly Pitched and Yawed Jets in Crossflow," *AIAA Journal*, Vol. 42, No. 5, 2004, pp. 874–882. doi:10.2514/1.2924

[15] Selby, G. V., Lin, J. C., and Howard. F. G., "Control of Low-Speed Turbulent Separated Flow Using Jet Vortex Generators," *Experiments in*

Fluids, Vol. 12, No. 6, 1992, pp. 394–400.
doi:10.1007/BF00193886

[16] Seifert, A., Darabi, A., and Wygnanski, I., "Delay of Airfoil Stall by Periodic Excitation," *Journal of Aircraft*, Vol. 33, No. 4, 1996, pp. 691–698.
doi:10.2514/3.47003

[17] Amitay, M., Smith, D. R., Kibens, V., Parekh, D. E., and Glezer, A., "Aerodynamic Flow Control over an Unconventional Airfoil Using Synthetic Jet Actuators," *AIAA Journal*, Vol. 39, No. 3, March 2001, pp. 361–370.
doi:10.2514/2.1323

[18] Mittal, R., Kotapati, R. B., and Cattafesta, L. N., "Numerical Study of Resonant Interactions and Flow Control in a Conical Separated Flow," 23rd AIAA Aerospace Sciences Meeting and Exhibit, AIAA Paper 05-1261, Jan. 2005.

[19] McManus, K. R., Legner, H. H., and Davis, S. J., "Pulsed Vortex Generator Jets for Active Control of Flow Separation," 25th AIAA Fluid Dynamics Conference, AIAA Paper 94-2218, June 1994.

[20] Nishri, B., and Wygnanski, I., "Effects of Periodic Excitation on Turbulent Flow Separation from a Flap," *AIAA Journal*, Vol. 36, No. 4, April 1998, pp. 547–556.
doi:10.2514/2.428

[21] Kumar, V., and Alvi, F. S., "Use of High-Speed Microjets for Active Separation Control in diffusers," *AIAA Journal*, Vol. 44, No. 2, Feb. 2006, pp. 273–281.
doi:10.2514/1.8552

[22] Yip, T. C. I., "Control of Flow Separation in Axial Compressors," 4th Year Project Report, Engineering Department, Univ. of Cambridge, Cambridge, England, U.K., 2006.

[23] Hiller, S. J., Hirst, M., Webster, J., Ducloux, O., Pernod, P., Touyeras, A., Garnier, E., Pruvost, M., Wakelam, C. T., and Evans, S. W., "ADVACT: An European Program for Actuation Technology in Future Aero-Engine Control Systems," 3rd AIAA Flow Control Conference, AIAA Paper 2006-3511, June 2006.

[24] Denton, J. D., "The 1993 IGTI Scholar Lecture: Loss Mechanisms in Turbomachines," *Journal of Turbomachinery*, Vol. 115, No. 4, 1993, pp. 621–656.
doi:10.1115/1.2929299

[25] Evans, S. W., "Flow Control in Compressors," Ph.D. Thesis, Univ. of Cambridge, Cambridge, England, U.K., 2009.

[26] Gad-el-Hak, M., "Flow Control: The Future," *Journal of Aircraft*, Vol. 38, No. 3, May–June 2001, pp. 402–418.
doi:10.2514/2.2796

[27] Honami, S., Shizawa, T., and Uchiyama, A., "Behavior of the Laterally Injected Jet in Film Cooling: Measurements of Surface Temperature and Velocity/Temperature Field Within the Jet," *Journal of Turbomachinery*, Vol. 116, No. 1, Jan. 1994, pp. 106–112.
doi:10.1115/1.2928264

F. Liu
Associate Editor